Proceedings of the ASME 2010 3rd Joint US-European Fluids Engineering Summer Meeting and 8th International Conference on Nanochannels, Microchannels, and Minichannels
FEDSM-ICNMM2010
August 1-5, 2010, Montreal, Canada

FEDSM-ICNMM2010-30697

IMMERSED BOUNDARY METHOD FOR LARGE EDDY SIMULATION AND LAGRANGIAN STOCHASTIC MODELING OF PASSIVE SCALAR DISPERSION DOWNSTREAM OF AN OBSTACLE

C. Le Ribault
LMFA, ECL, CNRS UMR 5509, UCB Lyon 1
36, avenue Guy de Collongue,
BP 163, 69131 Ecully Cedex, FRANCE
Email: catherine.le-ribault@ec-lyon.fr

S. Simoëns
LMFA, ECL, CNRS UMR 5509, UCB Lyon 1
36, avenue Guy de Collongue,
BP 163, 69131 Ecully Cedex, FRANCE
Email: serge.simoens@ec-lyon.fr

ABSTRACT

A large-eddy simulation (LES) using the atmospheric code ARPS is performed to study the passive scalar dispersion downstream of an obstacle. An immersed boundary method has been introduced to take into account the obstacle. To simulate the scalar dispersion, instead of resolving the passive scalar transport equation, fluid particles containing scalar are tracked in a Lagrangian way. The results of the LES are compared with the experiments of Vinçont et al. [1]. In those experiments, simultaneous measurements of the velocity and scalar concentration fields have been made in the plume emitting from a two-dimensional line source flushed with the wall. The source is one obstacle height downstream of a two-dimensional square obstacle located on the wall of a turbulent boundary layer. Our simulations predict the qualitative and quantitative features of the experimental results.

INTRODUCTION

The study of transport and mixing of reactant species such as fuel-oxidant mixing, contaminant dispersion, is very important for environmental problems. Considerable attention is paid to the prediction of concentration levels downwind of pollution sources, especially in the vicinity of one or more obstacle.

LES has become a well-established tool for the study of turbulent flows, the transport of passive scalars as well as the dispersion of reactive plumes. A large-eddy simulation (LES) combined with Lagrangian stochastic modeling at sub grid-scale level is used to study the passive scalar dispersion downstream of an obstacle. This model is integrated in the atmospheric code ARPS [2],[3].

The code ARPS is an atmospheric code and was not developed to deal with complicate geometries and blunt angles. Instead of using complicated boundary fitted grids to define the geometrical configuration, the immersed boundary method mimics a solid body by means of suitably defined body forces applied to the discretized set of the momentum equations [4]. Immersed boundary methods can broadly be categorized under two categories: first are methods that employ ”continuous forcing” wherein a forcing term is added to the Navier-Stokes equations. The main advantage of this category of methods is that they are formulated relatively independently of the spatial discretization and can therefore be implemented into an existing Navier-Stokes solver relatively simply. The second category consists in methods that employ ”discrete forcing” where the forcing is either explicitly or implicitly applied to the discretized Navier-Stokes equations. In this case the forcing scheme is much dependent on the spatial discretization scheme. The main advantage of this category of methods is that it allows a sharp representation of the immersed boundary. This is important for turbulent flows with boundary layers.

Experiments of the passive scalar dispersion from a line source downstream of an obstacle have been performed by Vinçont *et.* al. [1]. Those experimental data provide controlled

conditions necessary for testing prediction methods and models. They also give some insight into the underlying scalar transport processes. Our goal is to perform LES of this experiment and to compare with experimental results.

LARGE EDDY SIMULATION

The atmospheric code ARPS is used for the computation [2],[3]. ARPS is based on compressible Navier-Stokes equations describing the atmospheric flow. The governing equations of the atmospheric model component of ARPS include momentum, heat (potential temperature), mass (pressure), water subtances, turbuelent kinetic energy and the equation of state. The governing equations used are the result of direct transformation from the Cartesian system and are expressed in a fully conservative form. These equations are solved in a rectangular computational space. The discretized form of the governing equations can be found in [2],[3].

The Navier-Stokes equations in the LES approach are filtered. The top-hat filter with a filter width Δ is used. The effect of the subgrid scales are represented by the subgrid stress tensor $q_{ij} = \widetilde{u_i u_j} - \tilde{u}_i \tilde{u}_j$. $\tilde{u}_i$ is the filtered velocity and $i = 1,2,3$ refers to the x (streamwise), y (spanwise) and z (normal) directions respectively. This tensor is modeled by the Germano dynamic Smagorinsky model. For brevity, we do not repeat the equations for models of the subgrid stress tensor. A more complete description of the model can be found in [5], [6] .

COUPLING OF THE LAGRANGIAN STOCHASTIC SUBGRID MODEL WITH EULERIAN LES

Details of the coupling between the Eulerian LES and the Lagrangian stochastic subgrid model may be found in [7],[8]. Fluid particles are tracked in a Lagrangian way. The position of fluid particles at each timestep is given by:

$$\vec{x}_p(t) = \frac{d\vec{v}}{dt} \tag{1}$$

In a turbulent flow, the velocity of fluid particles may be obtained by:

$$v_i(t) = \tilde{u}_i(\vec{x}_p(t),t) + v_i'(t) \tag{2}$$

where v_i is the Lagrangian velocity of the fluid particle in the x_i direction and $\tilde{u}_i$ is the Eulerian velocity of the fluid at the position $\vec{x}_p(t)$ of the fluid particle. v_i' is the Lagrangian velocity fluctuation around the Eulerian large scale velocity $\tilde{u}_i$. In order to compute the movement of a fluid particle within a grid, a Langevin model is introduced:

$$\begin{cases} dx_{p_i} = v_i dt \\ dv_i = (\gamma_i + \alpha_{ij}(v_j - \tilde{u}_j(\vec{x}_p,t)))dt \\ \qquad\quad +\beta_{ij}\eta_j(t) \end{cases} \tag{3}$$

where $\eta_j(t)$ is an isotropic, Gaussian white noise with zero mean and variance dt, so that $\overline{\eta_i(t')\eta_j(t")} = \delta_{ij}\delta(t'-t")dt$. The velocity of each fluid particle at a given time t is modeled by a deterministic part $\gamma_i + \alpha_{ij}v_j'$ and a completely random term $\beta_{ij}\eta_j(t)$. The coefficients α_{ij}, β_{ij} and γ_i are determined by relating the subgrid statistical moments of $\vec{v}(t)$ to the filtered Eulerian moments of the fluid velocity. Knowing that the subgrid turbulence is assumed locally homogeneous and isotropic, the velocity of fluid elements given by the Lagrangian stochastic subgrid model can be writen as:

$$\begin{aligned} dv_i = [&\tfrac{\partial \tilde{u}_i}{\partial t} + \tfrac{\partial(\tilde{u}_i\tilde{u}_j)}{\partial x_j} + \tfrac{\partial \tau_{ij}}{\partial x_j} + \\ &\tfrac{3}{2}\tfrac{v_i - \tilde{u}_i}{\tilde{E}}\left(\tfrac{1}{3}\tfrac{d\tilde{E}}{dt} - \tfrac{C_o\tilde{\varepsilon}}{2}\right)]dt \\ &+\sqrt{C_o\tilde{\varepsilon}}\delta_{ij}\eta_j(t)dt \end{aligned} \tag{4}$$

where $\tilde{E}$ is the subgrid turbulent kinetic energy, C_o is the constant of Kolmogorov ($C_o = 2.1$) and $\tilde{\varepsilon}$ the dissipation rate of subgrid turbulent kinetic energy. Each fluid particle has a large-scale and a subgrid scale velocity component. The large-scale velocity of the fluid particle is directly computed by the LES. The subgrid scale velocity component is obtained from the subgrid scale closure. An additional transport equation is solved to obtain the residual kinetic energy $\tilde{E}$. The instantaneous rate of dissipation $\tilde{\varepsilon}$ is related to $\tilde{E}$ and the filter width Δ by:

$$\tilde{\varepsilon} = \frac{C_E\tilde{E}^{\frac{3}{2}}}{\Delta} \tag{5}$$

where the constant C_E is taken to be $C_E = 0.7$.

To take into account diffusion, a deterministic, continuous in time pairing particle exchange model is used.

IMMERSED BOUNDARY METHOD

The simulations are performed using the LES code ARPS 4.5.2. This is is a 3D, non-hydrostatic code where the fully compressible equations are solved with a time splitting procedure. The code ARPS is an atmospheric code and was not developed to deal with complicate geometries and blunt angles. Instead of using complicated boundary fitted grids to define the geometrical configuration, the immersed boundary method mimics a solid

body by means of suitably defined body forces applied to the discretized set of the momentum equations.

$$\frac{Du}{Dt} = -\frac{1}{\rho}\nabla p + \nu\nabla.[\nabla u] + F \tag{6}$$

The body force is imposed so that the velocity distribution on the immersed boundary is equal to a specified function V_s. The forcing will act on the points nearest to the immersed boundary. The source terms F can be computed by:

$$F = -Rhs + \frac{V_s - u^n}{\Delta t} \tag{7}$$

where *Rhs* represents the right-hand side of Eq. (6) without the body force F.

In the present paper, a new ghost-cell technique proposed by Ghias [9] for imposing the boundary conditions on the immersed boundaries has been implemented. This approach leads to a sharp representation of the immersed boundaries, a property that is especially useful for flow simulations at high Reynolds numbers with boundary layers. The velocity at the grid points external to the solid body is obtained by directly solving the Navier-Stokes equations. For the first point internal to the body, a ghost image is constructed by taking its symmetric to the boundary. The velocity at the ghost image location is evaluated using the value of the velocity at the solid wall and at the first external point if the ghost image is located between the wall and the first external point (figure 1). If the ghost image location is located between the two closest external grid points (figure 2), the velocity at those points is used.

Then the velocity at the internal node is computed by symmetry. In the corner, the scheme is slightly more complicated and the procedure is detailed in Ghias and al. Bilinear interpolations are used to estimate the velocity at the ghost image location in function of the adjacent grid points. This bilinear interpolation scheme in conjunction with the ghost cell results in second -order global as well as local spatial accuracy.

Zero pressure gradient boundary condition is also incorporated into the interpolation procedures to effectively reproduce the correct pressure distribution on the immersed boundaries and to enforce mass conservation (Li and Wang [10]). Those authors experiment that in the case of the cylinder, the calculation is not quite stable since the distribution is incorrect near the immersed boundary and that the problem is alleviated by the imposition of zero normal gradient condition of pressure. This approach can be interpreted as an alternative way to enforce continuity since the Poisson equation is derived from the continuity equation.

In our case, the construction of the immersed boundary is easy because the geometry is a simple rectangle.

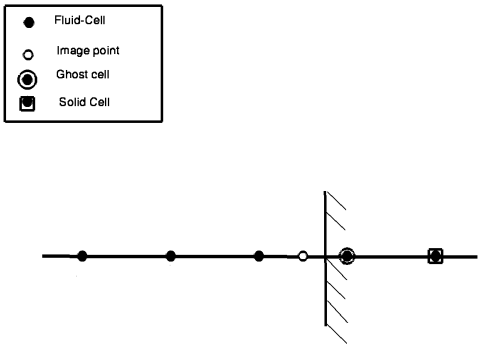

FIGURE 1. SKETCH OF THE INTERPOLATION PROCEDURE - THE IMAGE POINT IS LOCATED BETWEEN THE WALL AND THE FIRST EXTERNAL NODE

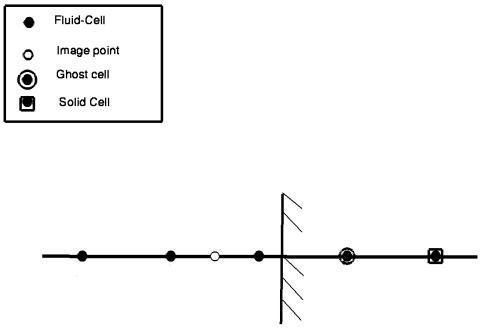

FIGURE 2. SKETCH OF THE INTERPOLATION PROCEDUCE - THE IMAGE POINT IS LOCATED BETWEEN THE TWO FIRST EXTERNAL NODES

In almost all of the reported works, staggered arrangement of variables on structured rectilinear grids were adopted. In ARPS, non staggered grids are used which require a separate treatment for each variable.

DESCRIPTION OF THE EXPERIMENTAL CASE AND COMPUTATIONAL PARAMETERS

Our aim is to validate our approach with the experiments of Vinçont [1] of scalar dispersion downstream of an obstacle in a turbulent boundary layer. In those experiments, simultaneous

measurements of the velocity and scalar concentration fields have been made. The scalar was emitted from a two-dimensional line source at the wall. The source is one obstacle height downstream of a two-dimensional square obstacle located on the wall of a turbulent boundary layer.

The dimensions of the computational domain in the streamwise, spanwise and wall-normal directions are respectively $l_x = 3.3L$, $l_y = 1.L$ and $l_z = 1.4L$, L being the boundary layer depth. The boundary layer depth L is equal to seven times the obstacle depth h. The number of nodes in each direction is respectively equal to $n_x = 250$, $n_y = 32$ and $n_z = 90$. The Reynolds number based on the obstacle height and the free stream velocity is equal to $Re_h = 1500$. The grid is uniform in the xy planes. In the z direction, the grid spacing is uniform until $y = 1.17h$ above the obstacle, then a slight stretching is applied using hyperbolic tangent function. The grid spacings are $\Delta_x = 0.013L$, $\Delta_y = 0.033L$ and $0.0033L < \Delta_z < 0.04L$. The no-slip boundary condition is applied at the wall. The immersed boundary method is applied on the obstacle. On the top of the domain and in the spanwise direction the mirror free-slip and the periodic boundary conditions are applied, respectively. In the streamwise direction, at the end of the domain the wave-radiation open boundary condition is used in order to allow acoustic waves in the interior of the domain to pass out freely through the boundary with minimal reflection. At the beginning of the domain, in the streamwise direction forcing is applied.

COMPUTATIONAL RESULTS

Streamlines of velocity

Before considering detailed statistical properties of the velocity field, instantaneous streamlines of the velocity (Figure 3) are presented.

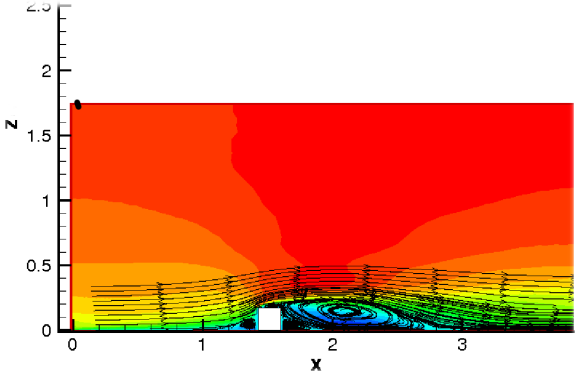

FIGURE 3. STREAMLINES OF VELOCITY

Upstream of the obstacle, a vortex with negative vorticity appears. Its characteristic size is approximately the same as the obstacle. Another vortex of about the same size with positive vorticity is seen just downstream the obstacle. A zone of high shear is evident above the obstacle with a region of some slow reverse flow between it and the obstacle. Downstream of the obstacle, a large recirculation region is apparent. The zone of the large recirculation is about 6 time the size h of the obstacle. In the experimental data the downstream end of the large recirculating region is around $6.5h$. In the present results, the point where the flow above the recirculating region reattaches to the wall appears to be at about $6.5h$. The computational value is then in the range of experimental values. In this region detailed experimental statistical information have been obtained at $4h$ and $6h$ downstream of the obstacle. The qualitative characteristics of the flow around the obstacle are in good agreement with experimental data. This mean velocity field indicates how the scalar from the source can be transported upstream and over the top of the obstacle.

Mean velocity field In figure 4 and 5, U/Ue profiles for the mean velocity components normalized by the external flow velocity Ue are shown respectively at the locations $4h$ and $6h$. The LES results are compared to the experimental results. A region of mean flow directed upstream is quite evident at $x = 4h$, up to above $0.6h$ above the wall. At $6h$ this reverse flow region is much smaller. The results are in overall agreements with experimental results. The size of the recirculation region is confirmed to be around $x = 6h$.

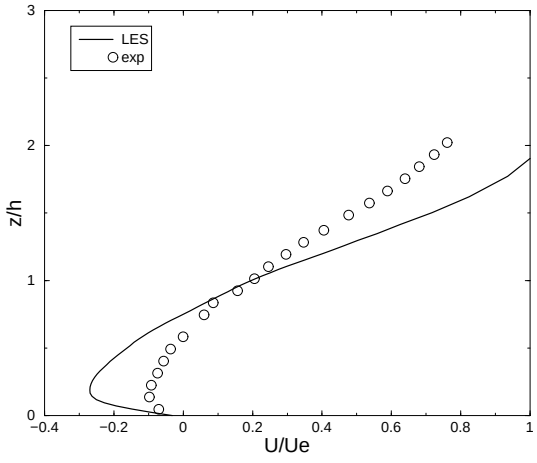

FIGURE 4. MEAN LONGITUDINAL U VELOCITY PROFILES DOWNSTREAM OF THE OBSTACLE AT $4h$

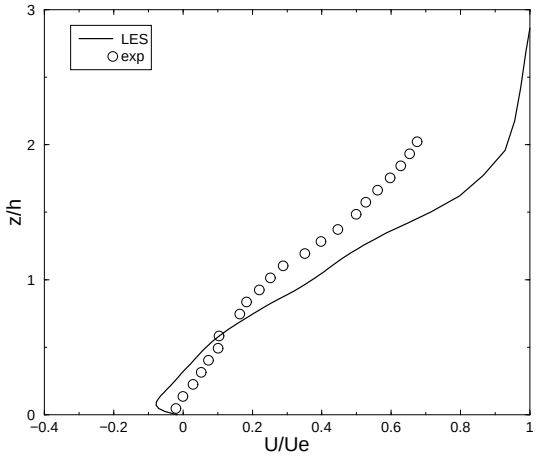

FIGURE 5. MEAN LONGITUDINAL U VELOCITY PROFILES DOWNSTREAM OF THE OBSTACLE AT 6h

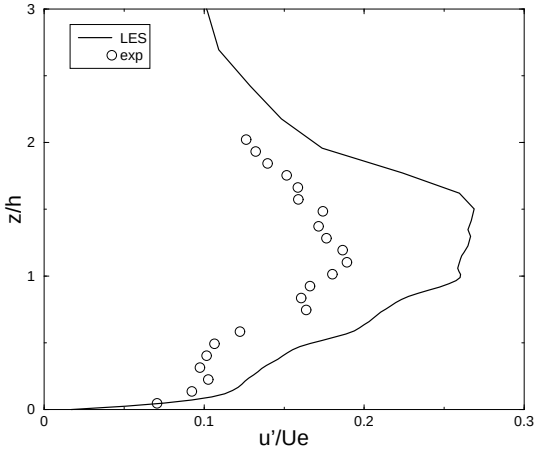

FIGURE 6. ROOT MEAN SQUARE LONGITUDINAL VELOCITY FLUCTUATION PROFILES DOWNSTREAM OF THE OBSTACLE AT 4h

Velocity turbulence intensities The root-mean square u'/Ue are shown in figure 6 and 7 at 4h and 6h downstream of the obstacle. The root-mean square of w'/Ue are also presented on the figures 8 and 9. The intensity of the w fluctuations is considerably less than the u fluctuations at both locations. The values predicted by the LES are higher than the experimental values. The maxima of the u'/Ue profiles occur in the vicinity of $1.2h - 1.5h$, in the mixing region above the level of the obstacle and near the inflection points of the $\overline{U}$ profiles where the mean velocity gradient is largest. The maxima of w'/Ue profiles also occur in the mixing region but are considerably less pronounced.

The Reynolds shear stress profiles for these two locations are respectively plotted on the figures 10 and 11. Like in the experimental results, $\overline{uv}/U_e^2$ values are everywhere negative and have larger magnitudes at the 6h location than at 4h for all y/h positions. The negative values indicate turbulent mixing in the recirculating bubble but stop above 2h which is the end of the obstacle wake. The negative maxima occur in the mixing zone just above the level of the top of the obstacle ($y/h \approx 1$).

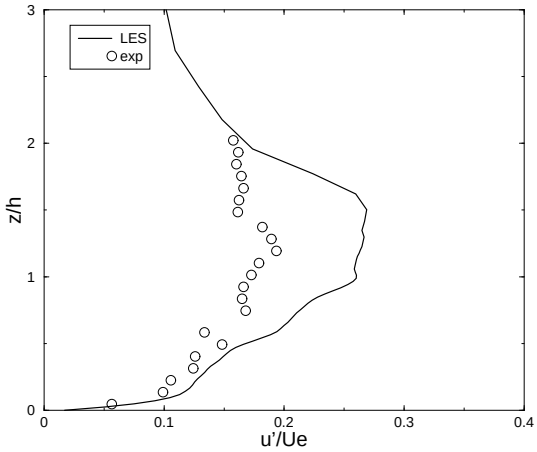

FIGURE 7. ROOT MEAN SQUARE LONGITUDINAL VELOCITY FLUCTUATION PROFILES DOWNSTREAM OF THE OBSTACLE AT 6h

CONCLUSION

An immersed boundary method has been introduced in the atmospheric code ARPS to study passive scalar dispersion downstream of an obstacle. Comparisons between LES and experimental field are performed on the mean and fluctuating velocity. Passive scalar results will be presented in a future paper. The immersed boundary method predicts the main qualitative and quantitative features of the experiments.

REFERENCES

[1] Vinçont J.Y, Simoëns S., Ayrault M., Wallace J.M. 2000, Passive scalar dispersion in a turbulent boundary layer from a line source at the wall and down stream of an obstacle. Journal of Fluid Mechanics, vol. 424, pp. 127-167.

[2] Xue M., Droegemeier K.K., Wong V. 2000, The advanced Regional Prediction System (ARPS) - A multi-scale nonhydrostatic atmospheric simulation and prediction model. Part I: model dynamics and verification, Meteorology and Atmospheric

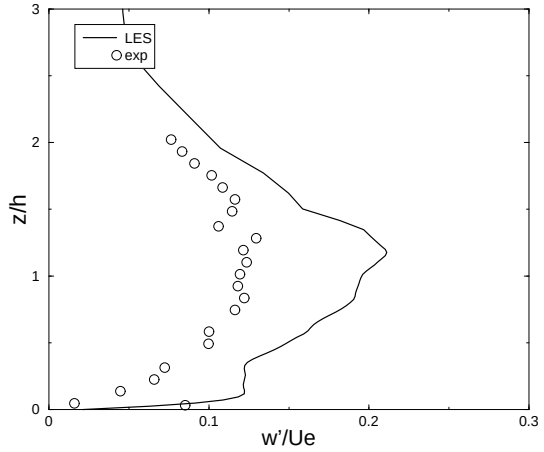

FIGURE 8. ROOT MEAN SQUARE WALL-NORMAL VELOCITY FLUCTUATION PROFILES DOWNSTREAM OF THE OBSTACLE AT 4*h*

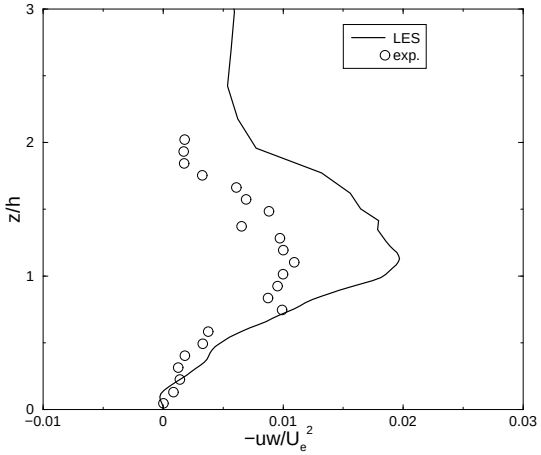

FIGURE 10. REYNOLDS SHEAR STRESS PROFILES DOWNSTREAM OF THE OBSTACLE AT 4*h*

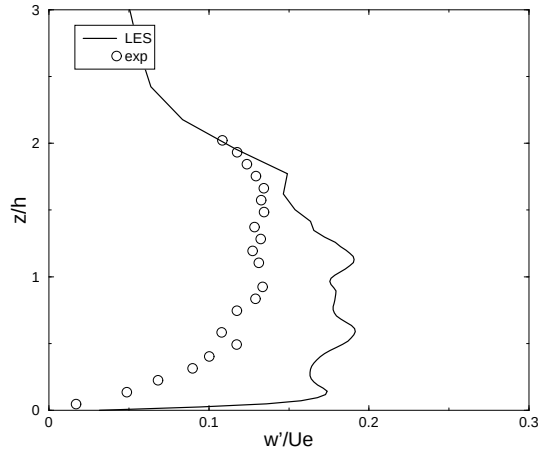

FIGURE 9. ROOT MEAN SQUARE WALL-NORMAL VELOCITY FLUCTUATION PROFILES DOWNSTREAM OF THE OBSTACLE AT 6*h*

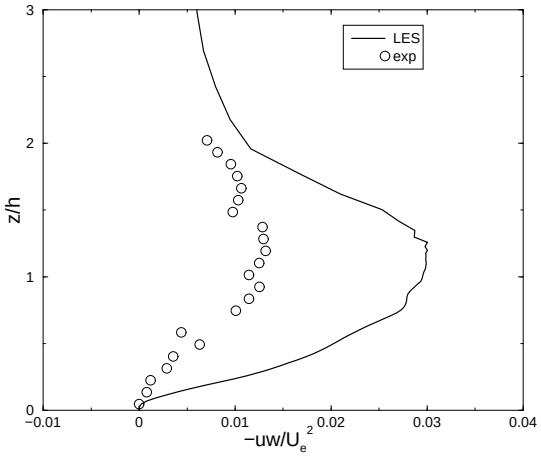

FIGURE 11. REYNOLDS SHEAR STRESS PROFILES DOWNSTREAM OF THE OBSTACLE AT 6*h*

Physics 75, pp. 161-193

[3] Xue M., Droegemeier K.K., Wong V., Shapiro A., Brewster K., Carr F., Weber D., Liu Y., Wang D. 2001, The advanced regional prediction system (ARPS) - a multi-scale nonhydrostatic atmospheric simulation and prediction tool. Part II: model physics and applications. Meteorology and Atmospheric Physics 76, pp. 143-165

[4] Mittal R., Iaccarino G. 2005, Immersed boundary methods, Annu. Rev. Mech. 37, pp. 239-261

[5] Vinkovic I., Aguirre C., Simoëns S. 2006, Large eddy simulation and Lagrangian stochastic modeling of passive scalar dispersion in a turbulent boundary layer. J. of Turbulence, vol. 7, n30, pp. 1-14.

[6] Vinkovic I., Aguirre C., Simoëns S.,Ayrault M. 2006, Large eddy simulation of the dispersion of solid particles in a turbulent boundary layer. Boundary Layer Meteoroly, vol. 121, pp. 283-311.

[7] Aguirre C., Brizuela A.B., Vinkovic I., Simoëns S. 2006, A subgrid Lagrangian stochastic model for turbulent passive and reactive scalar dispersion. Heat and Fluid Flow, vol. 27, pp. 627-

635.

[8] Vinkovic I., Aguirre C., Simoëns S., Gence J.N. 2005, Couplage d'un modèle stochastique lagrangien sous-maille avec une simulation grand es échelles, C. R. Mécanique 333, pp. 325-330.

[9] Ghias R., Mittal R., Dong H. (2007), A sharp interface immersed boundary method for compressible viscous flow, Journal of Computational Physics 225, pp. 528-553.

[10] Li C.W, WangL.L 2004, An immersed boundary finite difference method for LES of flow around bluff shapes, International Journal for Numerical methods in Fluids, vol. 46, pp. 85-107